HAL
open science

Optimized Si/SiO2 high contrast grating mirror design for mid-infrared wavelength range: robustness enhancement

Christyves Chevallier, Frédéric Genty, Joel Jacquet, Nicolas Fressengeas

To cite this version:

Christyves Chevallier, Frédéric Genty, Joel Jacquet, Nicolas Fressengeas. Optimized Si/SiO2 high contrast grating mirror design for mid-infrared wavelength range: robustness enhancement. Optics and Laser Technology, 2012, 44, pp.626-630. 10.1016/j.optlastec.2011.09.010 . hal-00628574

HAL Id: hal-00628574

https://centralesupelec.hal.science/hal-00628574v1

Submitted on 17 Nov 2011

HAL is a multi-disciplinary open access archive for the deposit and dissemination of scientific research documents, whether they are published or not. The documents may come from teaching and research institutions in France or abroad, or from public or private research centers.

L'archive ouverte pluridisciplinaire **HAL**, est destinée au dépôt et à la diffusion de documents scientifiques de niveau recherche, publiés ou non, émanant des établissements d'enseignement et de recherche français ou étrangers, des laboratoires publics ou privés.

Optimized Si/SiO_2 high contrast grating mirror design for mid-infrared wavelength range: robustness enhancement

C. Chevallier, F. Genty, J. Jacquet

Supélec, 2 rue Edouard Belin 57070 Metz, France

and

LMOPS, Laboratoire Matériaux Optiques, Photonique et Systèmes

Unité de Recherche Commune à l'Université Paul Verlaine - Metz et Supélec

N. Fressengeas

LMOPS, Laboratoire Matériaux Optiques, Photonique et Systèmes

Unité de Recherche Commune à l'Université Paul Verlaine - Metz et Supélec

November 17, 2011

Abstract

A high reflectivity and polarization selective high contrast grating mirror has been designed with the use of an automated optimization algorithm. Through a precise study of the tolerance of the different lengths of the structure, the robustness with respect to the fabrication errors has been enhanced to high tolerance values between 5 % and 210 %. This adjustment of the dimensions of the structure leads to a 250 nm large bandwidth mirror well adapted for a VCSEL application at $\lambda = 2.65$ µm and can easily be scaled for other wavelengths.

1 Introduction

The Tunable Diode Laser Absorption Spectroscopy (TDLAS) is a sensitive and fast method for gas sensing used for instance to measure concentrations of polluting gas such as CH_4 and CO. This technique requires the use of a tunable, stable and single mode operating source emitting in the mid infrared wavelength range beyond 2 µm where strong absorption lines are present for these gas [1, 2]. VCSELs are highly suitable for this kind of application, however, the development of continuous wave devices operating at room temperature at this wavelength range is still an important challenge.

Due to the small thickness of the gain region, VCSEL structures require high quality cavities with highly reflective Bragg mirrors (R > 99 %). In the mid-infrared wavelength range, even though the best performances were obtained with AlGaInAsSb material system, the relatively low index contrast ($\Delta n \sim 0.5$) between DBR layers make the mirrors become as thick as 11 µm impairing the electro-thermal-optical properties of the structure [3]. Currently, laser emission has been shown from an all-epitaxial monolithic microcavity near 2.3 µm in a continuous wave mode and in quasi-CW (5 %, 1 µs) up to 2.63 µm [4]. Another hybrid structure made of a dielectric top mirror and a buried tunnel junction operates in CW emission at room temperature in the 2.4-2.6 µm wavelength range [5].

One solution to increase the emission wavelength is the use of a high contrast grating mirror as top cavity mirror [6]. Such gratings, combined with a low index sub-layer, can exhibit high reflectivity of more than 99.9 % for bandwidths larger than 100 nm [7]. Moreover, due to their one dimensional symmetry, a high polarization selectivity can be performed by these mirrors and with a total thickness of less than 2 µm [8], the stability and quality of the VCSEL emitted beam should be improved.

However, contrary to Bragg mirrors, the explanation of the optical response of high contrast grating (HCG) is not straightforward and the design adjustment made in order to achieve the required properties for a VCSEL application is still complex. Even though several formalism have been defined, based for instance on the destructive interference of modes [9], the use of an optimization algorithm for the design combined with a numerical computation of the reflectivity keeps the advantage of versatility. Indeed, such a method easily allows the user to aim for specific properties of the HCG. It has been used for instance to design wide band and high diffraction efficiency grating [10], large bandwidth grating mirror for both TE and TM

polarization [11] or, like in this work, polarization selective large bandwidth mirror with technological constraints on the design dimensions [8].

In this work, we present a Si/SiO_2 HCG design optimized for a VCSEL application at $\lambda = 2.65$ µm. Then, through a precise study of the computed tolerances of the structure dimensions, the robustness is enhanced with respect to the fabrication errors.

2 Design of the HCG structure

The high contrast grating structure studied in this work is based on Si/SiO_2 materials which properties and fabrication process are well known. The grating is made of silicium (n = 3.435) on top of a low index layer of SiO_2 (n = 1.509) used to achieved high reflectivity [7] and allowing the use of a selective etching method for the fabrication of the grating. In order to increase the total reflectivity of the reflector and broaden the stopband, two quarter wavelength layers of Si/SiO_2 are combined with the grating [8]. For the simulation of the design, the substrate is chosen as the VCSEL cavity material with an optical index of n = 3.521.

In order to be well suitable for a VCSEL application, HCGs have to exhibit optical properties as we have defined with a 99.9 % transverse magnetic (TM) reflectivity for the largest possible bandwidth. Moreover, to ensure a polarization stability of the emitted beam, the reflectivity of the transverse electric (TE) mode has been chosen to be kept lower than 90 % for the whole bandwidth.

A 99.5 % TM reflectivity should be enough to achieve laser emission but a 0.4 % security margin has been chosen to account for possible experimental growth imperfections and losses due to absorption. Indeed, the presence of OH radicals as impurities in SiO_2 results in an absorption band in the 2.6-2.9 µm range [12]. In this reference, the absorption of silica has been measured with a 10 dB/cm value at 2.65 µm, i.e. the refractive index becomes $n_{SiO2} = 1.509 + 2.1e^{-4}j$, which results in a 0.1 % fall of the HCG reflectivity while a 0.4 % decrease of reflectivity has been observed for a simulation with a 20 dB/cm attenuation coefficient ($n_{SiO2} = 1.509 + 1.7e^{-3}j$) at 2.675 µm. This latter value appears therefore as the maximum absorption value allowed for the studied structure. However, the OH impurities concentration should strongly depends on the fabrication process and the exact value of the absorption must be determined in each case. For this theoretical

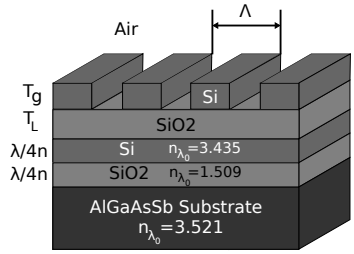

Figure 1: Scheme of the structure. The silicium grating defined by the empty length of the grooves L_e, the filled length L_f and the grating thickness T_g is on top of a SiO_2 layer of thickness T_L. These four parameters are adjusted to meet the characteristics of a VCSEL reflector.

study, a pure SiO_2 without any OH absorption was considered. Nevertheless, if the silica absorption is proven to be too high, this material can be replaced by another dielectric such as Si_3N_4.

The evaluation of the reflectivity of the mirror is made thanks to a rigorous coupled wave analysis (RCWA) [13, 14] which numerically finds an exact solution of Maxwell's equations for the electromagnetic diffraction problem of an infinite grating structure.

Reflection spectra for TE and TM modes are thus computed and through a well defined quality factor [8], the optical performance of the reflector is numerically evaluated. This performance is then maximized by a genetic optimization algorithm which searches for a global maximum of the quality factor by adjusting the design. The use of a global algorithm [15] is mandatory in this problem since the quality factor function exhibits numerous local maxima.

In this work, the performances of the grating are optimized by adjusting the empty and filled lengths (L_e and L_f), the grating thickness T_g and the sublayer thickness T_L as shown on Figure 1.

The use of an automated optimization presents the advantage of easily imposing technological constraints on the dimensions of the structure. These constraints have been set on the lengths L_e and L_f limited to a minimum value of 500 nm which should ease the photolithographic process. Besides, the etching process is also a critical step of the grating fabrication and, to achieve the theoretical grating profile presented on Figure 1, the shape factor $SF = L_e/T_g$ of the grooves is kept at a minimum value of 0.9 since squared patterns are easier to etch than deep ones.

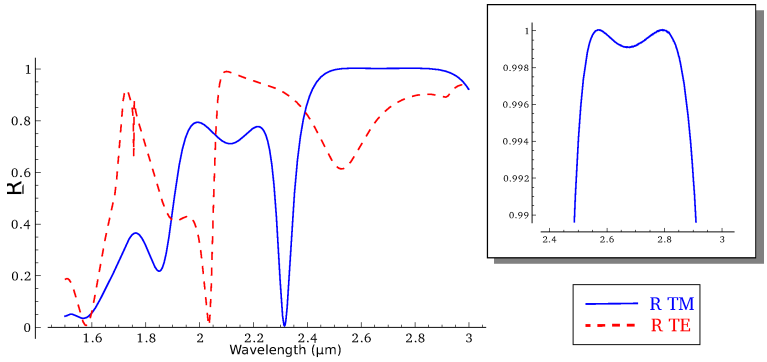

Figure 2: Reflection spectra for the TM mode (blue) and TE mode (dashed red) of the structure automatically optimized by a genetic-based algorithm. This optimum design exhibits a 307 nm large bandwidth with a 99.9 % high TM reflectivity.

The optimization for $\lambda = 2.65$ µm of the structure shown on Figure 1 results in a 307 nm large bandwidth mirror exhibiting a high polarization selectivity with $R_{TE} < 90$ % (Fig. 2). The optimum lengths of the design are given in Table 1 and satisfy the technological constraints with $L_e = 799$ nm, $L_f = 541$ nm and a shape factor $SF = 0.9$. The grating thickness $T_g = 886$ nm and the sublayer thickness $T_L = 321$ nm combined with the two quarter wavelength layers result in a 1.84 µm thick reflector. Even though the performances of this HCG are well adapted for a VCSEL application, the tolerances of the dimensions of this grating are critical. For instance, the 884 nm minimum grating thickness leads to a maximum error allowed as small as 2 nm.

3 Optimization of the robustness

The evaluation of the tolerances is performed by computing the variation range of one parameter for which the HCG keeps a 99.9 % TM reflectivity together with a $R_{TE} < 90$ % at $\lambda_0 = 2.65$ µm. This computation is made by varying one parameter at a time, for instance the grating thickness T_g, while keeping the other ones (T_L, L_e and L_f) constant at their optimal value.

The computation of the tolerances of the design found by the optimization algorithm exhibits large variation ranges of $\Delta L_e = 14$ %, $\Delta L_f = 25$ %, $\Delta T_g = 5$ % and $\Delta T_L = 68$ %. However, the optimum point is not centred in

Table 1: Tolerances of the optimum design found by the genetic-based algorithm.

	Optimum	Minimum	Maximum
L_e	799 nm	689 nm	803 nm
L_f	541 nm	495 nm	629 nm
T_g	886 nm	884 nm	932 nm
T_L	321 nm	196 nm	414 nm
$\Lambda = L_e + L_f$	1340 nm	1260 nm	1345 nm
$FF = L_f/\Lambda$	40.37 %	35.97 %	45.67 %
$\alpha_e = L_e + T_g$	1685 nm	1652 nm	1689 nm
$\beta_e = L_e/\alpha_e$	52.58 %	50.80 %	54.89 %
$\alpha_f = L_f + T_g$	1427 nm	1388 nm	1430 nm
$\beta_f = L_f/\alpha_f$	62.09 %	59.13 %	64.74 %

these variation ranges and the real tolerance values are much more limited with for instance a maximum increase of 4 nm on the empty length L_e. Moreover, these variation ranges are computed separately and give no information of the simultaneous error allowed on several parameters.

A solution to access this information is to compute the variation range of combinations of two dimensions. In the following, only (L_e, L_f), (L_e, T_g) and (L_f, T_g) combinations are evaluated since the sublayer thickness T_L is the most tolerant and centred parameter. Besides, T_L does not depend on the etching process and should be fabricated with a better accuracy than the grating parameters.

For the first couple (L_e, L_f), the variation ranges of two significant combinations of L_e and L_f are evaluated. The first one is the grating period given by $\Lambda = L_e + L_f$. This parameter is varied around its optimum value of $\Lambda = 1340$ nm while keeping the fill factor defined as $FF = L_e/\Lambda$ at its optimum value of 40.37 %. The second combination of L_e and L_f is the fill factor FF which variation range is evaluated with a constant grating period of Λ =1340 nm. Large tolerance values are exhibited by these parameters with 85 nm for $\Delta\Lambda$ and 9.7 % for ΔFF. The minimum and maximum of the

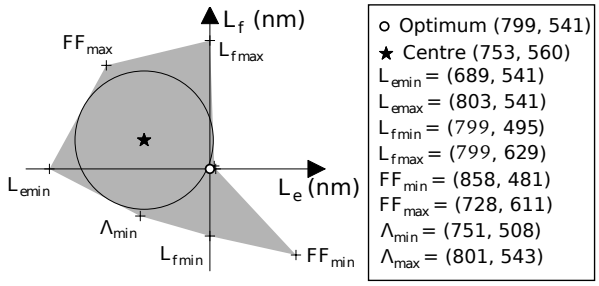

Figure 3: Tolerance map of L_e and L_f. The variation ranges of the grating period $\Lambda = L_e + L_f$ and the fill factor $FF = L_f/\Lambda$ define a polygon (grey) of allowed (L_e, L_f) couples for the design. The centre of the incircle ($\star$) enhances the robustness of the optimum point ($\circ$).

variation ranges of the four parameters L_e, L_f, Λ and FF, summarized in Table 1, creating eight (L_e, L_f) couples which can be plotted in a L_f versus L_e graph (Fig. 3). In the (L_e, L_f) plan, these points define a polygon, in grey on Figure 3, which area represents the tolerance area of (L_e, L_f) couples allowed for the design.

The representation of the tolerances in a (L_e, L_f) plan also shows very well the position of the optimum point within the tolerance area. In this case, the optimum point ($\circ$ on Figure 3) is located at an edge of the tolerance area ($L_e = 799$ nm, $L_f = 541$ nm). In order to increase the robustness regarding to the errors of fabrication which could be made on L_e and L_f, the design should be centred within the tolerance area. To do so, the centre of the largest incircle of the polygon representing the tolerance area is computed. This point is thus the farthest point from any edge of the polygon. The centre ($\star$) on Figure 3 corresponds to $L_e = 753$ nm and $L_f = 560$ nm and with a incircle radius of 47 nm, ensures a minimum tolerance of 94 nm on any combination of (L_e, L_f).

The second dimension couple studied is the empty length and grating thickness (L_e, T_g). In this case, both values of the optimum point (799, 886) are closed to the tolerance limit ($L_{e\ max} = 803$ nm, $T_{g\ min} = 884$ nm). This can easily be seen on Figure 4 where the optimum is localized at the edge of the tolerance area. In this map, the first combination of (L_e, T_g) is defined by $\alpha_e = L_e + T_g$ and the second one by $\beta_e = L_e/\alpha_e$. The polygon defined by the height extrema of the variation ranges of L_e, T_g, α_e and β_e (Table 1)

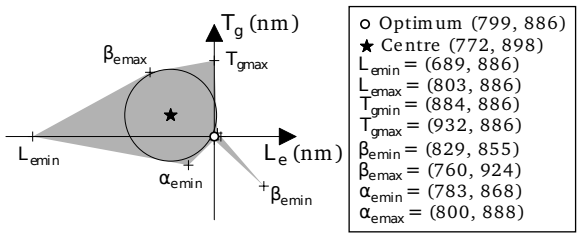

Figure 4: Tolerance map of L_e and T_g. The variation ranges of $\alpha_e = L_e + T_g$ and $\beta_e = L_e/\alpha_e$ define a polygon (grey) of allowed $(L_e,\ T_g)$ couples for the design. The centre of the incircle ($\star$) enhances the robustness of the optimum point ($\circ$).

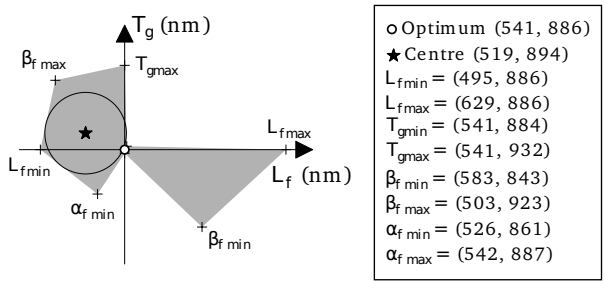

Figure 5: Tolerance map of L_f and T_g. The variation ranges of $\alpha_f = L_f + T_g$ and $\beta_f = L_f/\alpha_f$ define a polygon (grey) of allowed $(L_f,\ T_g)$ couples for the design. The centre of the incircle ($\star$) enhances the robustness of the optimum point ($\circ$).

exhibits an incircle with a radius of 28 nm centred at (772, 898) making a tolerance of a minimum value of 56 nm on the lengths (L_e, T_g) and any kind of their combinations.

The last couple, formed by the filled length L_f and grating thickness T_g, is optimized by computing the tolerance values of $\alpha_f = L_f + T_g$ and $\beta_f = L_f/\alpha_f$. As shown on Figure 5, the polygon exhibits two large areas joined by a very thin path where the optimum point is located at (541, 886). Once again, the optimum point is in a critical location closed to several edges of the tolerance area. By choosing the centre of the incircle of the polygon, located at (519, 894), variation ranges of the lengths L_f and T_g can be increased to a 44 nm value.

Table 2: Tolerances of the resulting design with optimized variation ranges.

	Optimum	Minimum	Maximum	
L_e	773 nm	703 nm	821 nm	(15 %)
L_f	541 nm	504 nm	608 nm	(19 %)
T_g	894 nm	870 nm	924 nm	(6 %)
T_L	321 nm	0 nm	674 nm	(210 %)

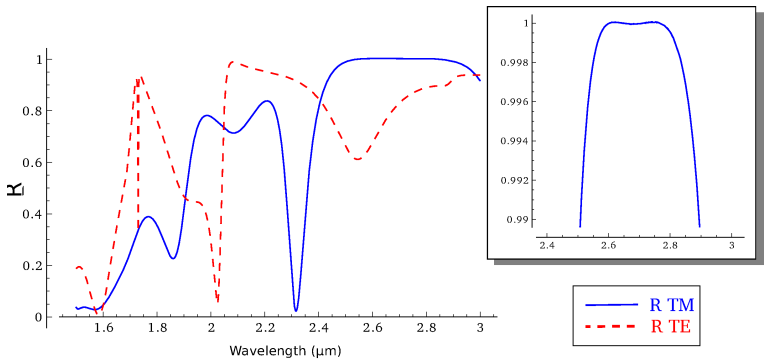

Figure 6: Reflection spectra for the TM mode (blue) and TE mode (dashed red) of the robust design with optimized tolerance values. This mirror exhibits a 250 nm large bandwidth for $R_{TM} > 99.9$ % and between 5 % and 210 % of tolerance on its dimensions.

4 Characteristics of the robust HCG

As a result of this optimization of the tolerances, three different designs are obtained. Each one is optimized to have the best tolerances for the couples (L_e, L_f), (L_e, T_g) and (L_f, T_g). These three points represent a triangle in a three dimensional space (L_e, L_f, T_g). Thus, to find a unique design with optimized tolerances, the centre of the incircle of this triangle has been computed and result in a final optimized design with lengths $L_e = 773$ nm, $L_f = 541$ nm and $T_g = 894$ nm. This structure exhibits a 250 nm large bandwidth as shown on Figure 6, which is 59 nm less than the optimum one found by the genetic-based algorithm. However, the computation of the variation ranges of the design dimensions (Table 2) exhibits a very robust design

with $\Delta L_e = 15\%$, $\Delta L_f = 19\%$, $\Delta T_g = 6\%$ and $\Delta T_L = 210\%$. Each optimum dimension of the structure is well centred within the variation ranges which would ease the fabrication process.

5 Conclusion

In this work, a Si/SiO_2 high contrast grating mirror has been designed for a VCSEL application at 2.65 µm. This mirror exhibits a 250 nm large bandwidth for $R_{TM} > 99.9$ % together with a strong polarization selectivity by keeping $R_{TE} < 90$ %. Moreover, with a total thickness of less than 2 µm, such reflector should improve the quality of the emitted laser beam of the VCSEL.

From a technological point of view, the fabrication constraints are respected with a large pattern resolution (> 500 nm) and a grating shape factor closed to 0.9. Moreover, the robustness with respect to the fabrication errors has been enhanced and leads to tolerance values larger than 5 % on the structure dimensions. Such characteristics make this HCG well adapted for a VCSEL application and should limit the pitfalls during the manufacturing process. Moreover, as spotted in [7], HCG can be scaled with wavelength in the limit of the refractive index dispersion.

Acknowledgements

The authors thank the French ANR for financial support in the framework of Marsupilami project (ANR-09-BLAN-0166-03) and IES and LAAS (France), partners of LMOPS/Supélec in this project. This work was also partly funded by the InterCell grant (http://intercell.metz.supelec.fr) by INRIA and Région Lorraine (CPER2007).

References

[1] J. Chen, A. Hangauer, R. Strzoda, M.-C. Amann, VCSEL-based calibration-free carbon monoxide sensor at 2.3 μm with in-line reference cell, Appl. Phys. B (2010) 1–910.1007/s00340-010-4011-0. doi:10.1007/s00340-010-4011-0.
URL `http://dx.doi.org/10.1007/s00340-010-4011-0`

[2] G. Boehm, A. Bachmann, J. Rosskopf, M. Ortsiefer, J. Chen, A. Hangauer, R. Meyer, R. Strzoda, M.-C. Amann, Comparison of InP- and GaSb-based VCSELs emitting at 2.3μm suitable for carbon monoxide detection, Journal of Crystal Growth 323 (1) (2011) 442 – 445, proceedings of the 16th International Conference on Molecular Beam Epitaxy (ICMBE). doi:DOI: 10.1016/j.jcrysgro.2010.11.174.
URL `http://www.sciencedirect.com/science/article/pii/S0022024810011735`

[3] L. Cerutti, A. Ducanchez, G. Narcy, P. Grech, G. Boissier, A. Garnache, E. Tournié, F. Genty, GaSb-based VCSELs emitting in the mid-infrared wavelength range (2-3 μm) grown by MBE, J. Cryst. Growth 311 (7) (2009) 1912–1916. doi:DOI: 10.1016/j.jcrysgro.2008.11.026.

[4] A. Ducanchez, L. Cerutti, P. Grech, F. Genty, E. Tournié, Mid-infrared GaSb-based EP-VCSEL emitting at 2.63 μm., Electron. Lett. 45 (5) (2009) 265–267.

[5] A. Bachmann, S. Arafin, K. Kashani-Shirazi, Single-mode electrically pumped GaSb-based VCSELs emitting continuous-wave at 2.4 and 2.6 μm, New J. Phys. 11 (12) (2009) 125014.
URL `http://stacks.iop.org/1367-2630/11/i=12/a=125014`

[6] M. Huang, Y. Zhou, C. Chang-Hasnain, A surface-emitting laser incorporating a high-index-contrast subwavelength grating, Nat. Photon. 1 (2) (2007) 119–122. doi:10.1038/nphoton.2006.80.
URL `http://dx.doi.org/10.1038/nphoton.2006.80`

[7] C. Mateus, M. Huang, Y. Deng, A. Neureuther, C. Chang-Hasnain, Ultrabroadband mirror using low-index cladded subwavelength grating, IEEE Photon. Technol. Lett. 16 (2) (2004) 518–520. doi:10.1109/LPT.2003.821258.

[8] C. Chevallier, N. Fressengeas, F. Genty, J. Jacquet, Optimized subwavelength grating mirror design for mid-infrared wavelength range, Appl. Phys. A- Mater. 103 (4) (2011) 1139–1144. doi:10.1007/s00339-010-6059-4.

[9] V. Karagodsky, F. G. Sedgwick, C. J. Chang-Hasnain, Theoretical analysis of subwavelength high contrast grating reflectors, Opt. Express 18 (16) (2010) 16973–16988. doi:10.1364/OE.18.016973.

[10] J. Wang, Y. Jin, J. Shao, Z. Fan, Optimization design of an ultrabroadband, high-efficiency, all-dielectric grating, Opt. Lett. 35 (2) (2010) 187–189. doi:10.1364/OL.35.000187.
URL http://dx.doi.org/10.1364/OL.35.000187

[11] M. Shokooh-Saremi, R. Magnusson, Wideband leaky-mode resonance reflectors: Influence of grating profile and sublayers, Opt. Express 16 (22) (2008) 18249–18263. doi:10.1364/OE.16.018249.
URL http://www.opticsexpress.org/abstract.cfm?URI=oe-16-22-18249

[12] R. A. Soref, S. J. Emelett, W. R. Buchwald, Silicon waveguided components for the long-wave infrared region, Journal of Optics A: Pure and Applied Optics 8 (10) (2006) 840.
URL http://stacks.iop.org/1464-4258/8/i=10/a=004

[13] H. Rathgen, mrcwa 20080820, http://mrcwa.sourceforge.net/ (February 2010).

[14] M. G. Moharam, D. A. Pommet, E. B. Grann, T. K. Gaylord, Stable implementation of the rigorous coupled-wave analysis for surface-relief gratings: enhanced transmittance matrix approach, J. Opt. Soc. Am. A 12 (5) (1995) 1077–1086.
URL http://josaa.osa.org/abstract.cfm?URI=josaa-12-5-1077

[15] D. L. Kroshko, OpenOpt 0.27, http://openopt.org/ (December 2009).

List of Figures

1 Scheme of the structure. The silicium grating defined by the empty length of the grooves L_e, the filled length L_f and the grating thickness T_g is on top of a SiO_2 layer of thickness T_L. These four parameters are adjusted to meet the characteristics of a VCSEL reflector. 4

2 Reflection spectra for the TM mode (blue) and TE mode (dashed red) of the structure automatically optimized by a genetic-based algorithm. This optimum design exhibits a 307 nm large bandwidth with a 99.9 % high TM reflectivity. 5

3 Tolerance map of L_e and L_f. The variation ranges of the grating period $\Lambda = L_e + L_f$ and the fill factor $FF = L_f/\Lambda$ define a polygon (grey) of allowed (L_e, L_f) couples for the design. The centre of the incircle ($\star$) enhances the robustness of the optimum point ($\circ$). 7
4 Tolerance map of L_e and T_g. The variation ranges of $\alpha_e = L_e + T_g$ and $\beta_e = L_e/\alpha_e$ define a polygon (grey) of allowed (L_e, T_g) couples for the design. The centre of the incircle ($\star$) enhances the robustness of the optimum point ($\circ$). 8
5 Tolerance map of L_f and T_g. The variation ranges of $\alpha_f = L_f + T_g$ and $\beta_f = L_f/\alpha_f$ define a polygon (grey) of allowed (L_f, T_g) couples for the design. The centre of the incircle ($\star$) enhances the robustness of the optimum point ($\circ$). 8
6 Reflection spectra for the TM mode (blue) and TE mode (dashed red) of the robust design with optimized tolerance values. This mirror exhibits a 250 nm large bandwidth for $R_{TM} > 99.9$ % and between 5 % and 210 % of tolerance on its dimensions. 9

List of Tables

1 Tolerances of the optimum design found by the genetic-based algorithm. 6
2 Tolerances of the resulting design with optimized variation ranges. 9